CHEMISTRY OF MATERIALS

ARTICLE

pubs.acs.org/cm

New $(Bi_{1.88}Fe_{0.12})(Fe_{1.42}Te_{0.58})O_{6.87}$ Pyrochlore with Spin-Glass Transition

Gunda Santosh Babu,[†,‡] Matjaz Valant,[†,*] Katharine Page,[§] Anna Llobet,[§] Taras Kolodiazhnyi,[⊥] and Anna-Karin Axelsson[#]

[†]Materials Research Laboratory, University of Nova Gorica, Vipavska 13, 5000 Nova Gorica, Slovenia.

[§]Lujan Neutron Scattering Center, Los Alamos National Laboratory, Los Alamos, New Mexico 87545, United States

[⊥]National Institute for Materials Science, 1-1 Namiki, Tsukuba, Ibaraki 305-0044, Japan.

[#]Department of Materials, Imperial College London, South Kensington Campus, London SW7 2AZ, United Kingdom

Supporting Information

ABSTRACT: The synthesized $(Bi_{1.88}Fe_{0.12})(Fe_{1.42}Te_{0.58})O_{6.87}$ is characterized with so far the highest Fe content among pyrochlores. Consequently, it exhibits a strong spin-glass magnetic transition at around 20 K. The dielectric relaxation in the same temperature range originates from multiwall hopping of the displaced ions on A and O′ sites. The displacement was confirmed with the structural analysis of the pyrochlore using Rietveld refinement on joint neutron and X-ray diffraction data. At room temperature, the pyrochlore exhibits a cubic $Fd\bar{3}m$ symmetry (a = 10.38804 (13) Å) with Fe^{3+} ions sharing A and B structural sites. The refined results indicate on a displacive disorder with A-site positioned at 96g and O′ positioned at 32e. The lattice vibrational analysis using Raman spectra is in agreement with the displacive disorder of the pyrochlore.

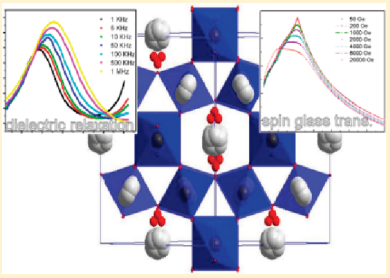

KEYWORDS: Bi-pyrochlore, displacive disorder, Raman spectra, dielectric relaxation, spin glass

INTRODUCTION

Pyrochlore structure, represented by the general formula $A_2B_2O_7$ or $A_2O'\cdot B_2O_6$, can accommodate a wide range of different chemical constituents and structural defects, which makes functional properties of pyrochlores versatile and interesting for technological such as applications microwave device technologies, radioactive waste materials, photocatalysis, thermistors, varistors, gas sensors, switching elements and resistors, etc.[1−4] A popular member from this group of materials is $(Bi_{1.5}Zn_{0.5})(Nb_{1.5}Zn_{0.5})O_6O'$, which exhibits a high dielectric constant. It remains paraelectric down to lowest temperatures[5,6] and it was reported that the good dielectric properties are also retained for the thin films.[7]

Interesting magnetic properties such as long-range antiferromagnetic/ferromagnetic ordering and short-range ordering, such as spin-glass, spin ice and spin liquid type of ordering, were well-studied in rare-earth-based pyrochlores.[8] Recently Bi−Fe−Nb-O[9] and Bi−Co−Nb−O[10] pyrochlores were reported to exhibit paramagnetic behavior with antiferromagnetic interactions at cryogenic temperatures. Antiferromagnetic interactions were also suggested for $Bi_2Pt_{1.5}Fe_{0.5}O_7$ and Bi_2NbFeO_7 pyrochlores;[11] however, no evidence of long-range antiferromagnetism was provided for $Bi_2Pt_{1.5}Fe_{0.5}O_7$. Later detailed studies[9] on Bi_2O_3: Fe_2O_3: Nb_2O_5 system showed that Bi_2NbFeO_7 is a three-phase mixture instead of a single-phase pyrochlore. Both of the above materials contain Bi^{3+} and Fe^{3+} ions similar to the widely studied $BiFeO_3$ perovskite with simultaneous existence of ferroic properties (multiferroic). Antiferromagnetism in $BiFeO_3$ is due to Fe^{3+} super exchange interactions and ferroelectricity is due to lone pair of Bi^{3+} ion.[12] It is reported that partial covalency of Fe 3d and O 2p orbitals is another factor that contributes to induction of ferroelectricity in $BiFeO_3$.[13] Ferroelectricity is rare in pyrochlore materials but recently it was confirmed for $Cd_2Nb_2O_7$ by Weller et al.[14] with Rietveld refinement of high resolution neutron diffraction data. They reported that below 180 K temperature $Cd_2Nb_2O_7$ pyrochlore undergoes a structural transition from the room temperature cubic $Fd\bar{3}m$ to the low-temperature tetragonal $I\bar{4}m2$ symmetry.

The ideal structural arrangement of the pyrochlore with $Fd\bar{3}m$ cubic symmetry consists of A and B atoms that occupy 16d (0.5, 0.5, 0.5) and 16c (0, 0, 0) special positions, respectively, whereas O and O′ atoms occupy nonequivalent crystallographic sites 48f (x, 0.125, 0.125) and 8b (0.375, 0.375, 0.375), respectively. In the pyrochlore structure, A_2O' chains weakly interact with the more rigid B_2O_6 network. Therefore, cation and/or anion vacancies in the A_2O' network of defect pyrochlores do not significantly reduce the stability of the lattice. Displacive disorder in the A_2O' is observed in rare-earth-based pyrochlores such as $La_2Zr_2O_7$[15] but it is also often encountered in Bi-based pyrochlores[9,10,16] where it is attributed to the stereochemically active lone electron pair of Bi^{3+} ion.[17,18] Studies of the local structure of Bi−Zn/Fe−Nb−O pyrochlores by Krayzman et al.[19] revealed that the displacement directions of the A-site ions are determined by

Received: January 27, 2011
Revised: March 29, 2011
Published: April 18, 2011

Table 1. 300 K Refinement Results of Two Models Described in the Text: O′ on 8*b* and 32*e* site[a]

atom	*x*	*y*	*z*	site	occ.	U_{iso}(Å^2)
Bi/Fe	0.47280(20)	0.51403(20)	0.51403(20)	96*g*	0.155(3)/0.014(3)	0.02274(25)
	0.47240(20)	**0.51366(22)**	**0.51366(22)**	**96*g***	**0.158(2)/ 0.012(3)**	**0.02281(26)**
Fe/ Te	0	0	0	16*c*	0.707(2)/0.293(2)	0.00545(8)
	0	**0**	**0**	**16*c***	**0.708(2)/ 0.292(2)**	**0.00542(8)**
O	0.322394(21)	0.125	0.125	48*f*	1.0	0.01330(8)
	0.322691(21)	**0.125**	**0.125**	**48*f***	**1.0**	**0.01329(8)**
O′	0.375	0.375	0.375	8*b*	0.964(3)	0.04818(37)
	0.3848(5)	**0.3848(5)**	**0.3848(5)**	**32*e***	**0.240(1)**	**0.037(1)**

[a] Model with O′ ion sitting on 32*e* site is in bold letters. Standard deviations in parentheses are described only for the refined parameters. Lattice constant obtained is 10.38807(13) Å/**10.38804(13) Å**.

nature of A-site cations and the local B-site configurations. Avdeev et al.[20] noted that the off-centering of the A-site cations can also occur when the A-site is occupied by small transition-metal ions, because the A-site cavity is too big for them to maintain the ideal central position. This was further supported by the recent study on Ca−Ti−(Nb,Ta)−O pyrochlores.[21] These pyrochlores exhibited a substantial displacive disorder without presence of lone electron pairs but with smaller Ti^{4+} ions on the A-site. Vanderah et al.[22] reported that a pyrochlore structure can accommodate up to 25% of small B cations on its A-site by the displacive disorder. Because large A cations and small B cations are electronically dissimilar, electric and magnetic properties can be modeled by mixing them in A_2O' network. Because of misplacement of the smaller B-site ions onto the A-site and displacement of the A-site and O′ ions from their ideal positions, these pyrochlores are termed as misplacive displaced pyrochlores.

In the quest for the new magnetic pyrochlores with potential magnetoelectric coupling, magnetoresistance or dilute magnetic semiconductor characteristics we have focused on the Bi_2O_3−Fe_2O_3−TeO_3 system to explore pyrochlores with the highly polarizable Bi^{3+} cation and the magnetic Fe^{3+} cation in combination with Te^{6+} cation. Because of its high valence state, Te^{6+} facilitates accommodation of a high Fe^{3+} content into the pyrochlore, which is expected to result in a spin ordering. Within this study, we have discovered a new pyrochlore composition with spin-glass transtion. We report on its synthesis, structure characterization, Raman spectra analysis, and dielectric and magnetic properties.

EXPERIMENTAL SECTION

Pyrochlore samples were prepared by the solid state reaction method using initial reagents Bi_2O_3 (Alfa Aesar, 99.975%), TeO_2 (Alfa Aesar, 99.99%) and Fe_2O_3 (Alfa Aesar, 99.945%). Stoichiometric powders were mixed in an agate mortar with ethanol for 30 min. Pelletized powders were heated in two steps in oxygen atmosphere, first at 530 °C for 5 h and subsequently at 840 °C for 5 h with intermediate grinding. Sintering of uniaxial pressed pellets was carried out in air at 880 °C for 3 h. The samples were mirror polished on one side for Raman spectroscopy.

X-ray diffraction data were collected using PANalytical X'pert pro MPD in Bragg−Brentano geometry with X'Celerator detector. The collection conditions were CuK_α-radiation, 40 kV 40 mA, 0.025° step scan, 0.5° divergence slit and 0.02 rad incident and receiving soller slits. Time-of-flight neutron diffraction (ND) data was collected on the HIPD instrument at the Lujan Neutron Scattering Center at Los Alamos National Laboratory at temperatures between 4 and 300 K. 8 g of powder were loaded in vanadium sample cans for the measurement. A Rietveld refinement of the room temperature data was performed jointly on 6 banks of neutron data and X-ray data set using the GSAS suite with EXPGUI.[23,24]

Raman measurements were taken using a Renishaw RM-2000 CCD spectrometer equipped with a 514 nm laser together with a 514 nm edge filter and an additional cutoff of 30 cm^{-1} filter for allowance of low wave numbers. Spectra were obtained using a 50× long working distance objective, which allowed the laser to be focused on to the samples surface to a spot size of approximately < 2 μm. The Raman spectra were analyzed using FOCUS software.[25] The Raman spectrum was divided with Bose−Einstein thermal factor[26] and then least-squares fitted using sum of Lorentzian curves. For low temperature dielectric measurements, pellets were silver coated on both sides and mounted in the closed-cycle cryocooler. The data was collected from 1 kHz to 1 MHz using a high precision LCR meter (Agilent E4980A). Magnetic moments of the powder samples in the 2−300 K range were measured using superconducting quantum interference device (Quantum Design, MPMS, USA).

X-ray and Neutron Diffraction Analysis. During the investigation of Bi_2O_3−Fe_2O_3−TeO_3 system, a pyrochlore phase that has never been reported earlier was synthesized. The nominal molar oxide ratio of the synthesized pyrochlore was Bi_2O_3:Fe_2O_3:TeO_3 = 1.0:0.936:0.751. Although X-ray only data indicated on single-phase composition, neutron diffraction showed the existence of a very small α-Fe_2O_3 impurity (∼1.88 ± 0.04 wt %) that was accounted for in the joint refinements. This impurity should not affect our analysis of the magnetic properties of the matrix phase because below the Morin spin-reorientation transition at around 263 K, the α-Fe_2O_3 does not show any magnetic transition that can be interfering with the observed low-temperature susceptibility curves of the pyrochlore phase.

Except the (442) reflection, observed in the X-ray powder pattern at 2θ = 52.789°, all other reflections are allowed in an ideal undistorted pyrochlore structure with the cubic $Fd\bar{3}m$ symmetry. The presence of the (442) reflection can be rationalized by a displacement of the A-site atom from its ideal (0.5, 0.5, 0.5) position of 16*d*, to a lower-symmetry position.[16,27] Similar to refinements on a number of other reported misplaced displacive pyrochlores[9,10,16,20] a model with displaced A ion was selected to refine the XRD and ND patterns of the new pyrochlore and during the refinement smaller Fe^{3+} was allowed to occupy A site position. Refinement with Bi/Fe at *96 g* and O′ ion at *8b* position

Table 2. List of Displacements for A and O′ Ions and Percentage of B Site Ions on a Site in Misplaced-Displacive Pyrochlores[a]

pyrochlore	displacement of A site ion (Å)	displacement of O′ ion (Å)	percentage (%) of B-site ion on A-site
$(Bi_{1.88}Fe_{0.12})(Fe_{1.42}Te_{0.58})O_{6.87}$	0.35	0.18	6 (Fe)
Bi−Fe−Nb−O[12]	0.43	0.22	9.5 (Fe)
Bi−Zn−Nb−O[29]	0.39	0.34	16 (Zn)
Bi−Co−Nb−O[13]	0.34	0.45	22 (Co)
Ca−Ti−Nb−O[20]	0.7[b]	0.48	24.5(Ti)

[a] Ion type in the last column is given in parentheses. In all the cases, O′ ion was displaced to 32*e* position. [b] In Ca−Ti−Nb-O, only Ti^{4+} occupying A site is displaced by 0.7 Å.

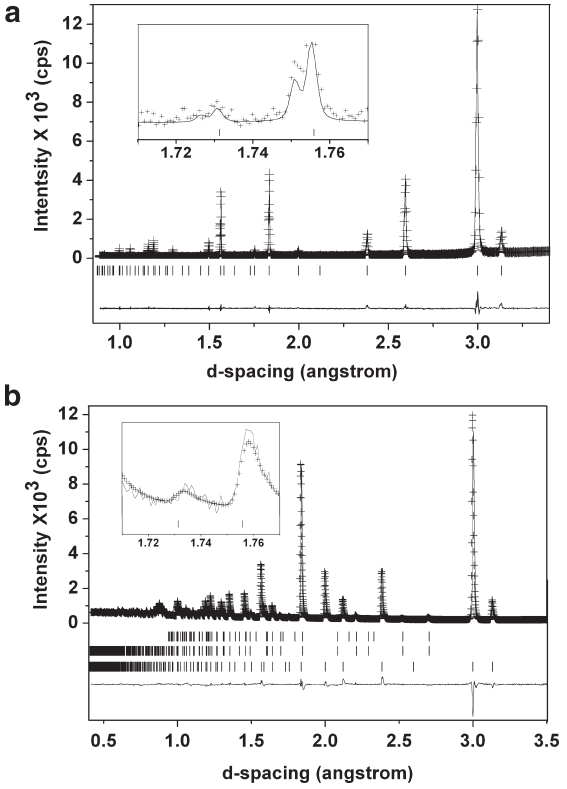

Figure 1. (a) 300 K Rietveld XRD refinement fit and (b) the fit of 153° bank 1 neutron TOF spectra of $(Bi_{1.88}Fe_{0.12})(Fe_{1.42}Te_{0.58})O_{6.87}$. Observed (+ marks), calculated (solid line) and difference (below) patterns are shown. Tick marks at (a) and bottom (b) are for the pyrochlore, middle (b) the nuclear structure of Fe_2O_3 impurity, and top (b) the magnetic structure of Fe_2O_3 impurity.

resulted $\chi^2 = 15.29$ and $R_{wp} = 0.0251$ with O′ thermal parameter of 0.46 Å^2. In the next step, O′ ion was refined with *32e* position, which resulted in $\chi^2 = 15.36$ and $R_{wp} = 0.0252$ with decreased O′ thermal parameter of 0.37 Å^2. The model with O′ ion at *32e* position slightly increased discrepancy factors but improved thermal parameter of O′. Any other choice of displacement of O′ ion in $Fd\bar{3}m$ symmetry worsened the refinement. The final refinement results are presented in Table 1.

The misplacement of smaller B-site ions to the A site in the bismuth pyrochlores is expected to result in a displacement of O′ ion to achieve chemically reasonable bond distances.[16,28] The correlation of O′ ion displacement and A-site occupancy of smaller ions (e.g., Fe, Co and Zn) has already been observed.[9,10,22] The present refinement result with O′ ion at *32e* site shows that ~6% of the A-sites is occupied by Fe^{3+} and O′ is displaced by 0.18 Å. As it is shown in the Table 2 these perfectly corresponds to the values and trends observed for other similar bismuth pyrochlores. In addition, the neutron diffraction refinement on

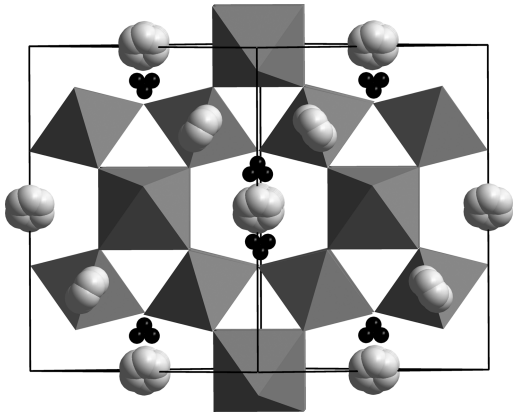

Figure 2. Crystal structure of the displacive disordered $(Bi_{1.88}Fe_{0.12})$-$(Fe_{1.42}Te_{0.58})O_{6.87}$ pyrochlore projected close to (110) direction. The corner-connected octahedra represent $(Fe_{1.42}Te_{0.58})O_6$ substructure. The toroids of flat ellipsoids represent six equivalent 96*g* A-site $(Bi_{1.88}Fe_{0.12})$ and black ellipsoids represent O′ atoms at 32*e* site.

$Bi_2Ti_2O_7$, where there is no misplacement of B-site ion to A-site, indicated that O′ ion occupies mixture of 32*e* and 8*b* positions[29] with only about 3% at 32*e* position. Recent in depth local structure studies on $Bi_2Ti_2O_7$ showed that the O′ ion position distribution is densely centered on the ideal 8*b* position.[18] This supports the observed correlation that in the absence of the misplacement, i.e., smaller B-site ion on A-site, O′ ion sits on the ideal position (8*b*) in the pyrochlores structure.

In the previous work, the model describing displacement along (111) direction (i.e., 32*e* position for O′) was finally chosen for Bi−Zn−Nb-O pyrochlore based on the crystal chemistry requirements despite convergence of neutron refinement with all other choices of O′ ion in $Fd\bar{3}m$ symmetry.[30] All these results corroborate that the model with O′ ion at 32*e* position correctly describes these pyrochlore. Based on the refinement and considering the stoichiometric constrains for pyrochlores the formula of this pyrochlore can be, within the analytical error bars from Table 1, written as $(Bi_{1.88}Fe_{0.12})(Fe_{1.42}Te_{0.58})O_{6.87}$ (hereafter BFT). The diffraction and refined profiles are shown in Figure 1.

The results of the refinement show that the $(Fe/Te)O_6$ octahedra are nearly regular with metal oxygen bond lengths of 1.98560(8) Å and O−Fe/Te-O angles deviated by 4 from 90°. The bond valence sum for Fe/Te atoms at 16*c* site using the occupancy factors in Table 1 is 3.76 v. u., which agrees well with the bond valence sum of 3.87 v.u., calculated using formal valences of ions. The structure of the displaced pyrochlore is presented in Figure 2.

Raman Spectra. According to a factor group analysis, there are 6 Raman active modes $(A_{1g} + E_g + 4F_{2g})$, 7 F_{1u} infrared-active modes and 1 F_{1u} acoustic mode for a cubic $Fd\bar{3}m$ pyrochlore with an ideal setting (i.e., without any displacement of A and O′ from their ideal sites).[31] In this ideal setting of the pyrochlore, the Raman modes are only due to

dx.doi.org/10.1021/cm200281z |*Chem. Mater.* 2011, 23, 2619–2625

B_2O_6 sublattice dynamics whereas in the displaced pyrochlore structures the relaxation of the selection rules can result in appearance of more Raman modes, including some infrared vibrational modes.[26]

The Raman modes of the BFT pyrochlore, which are presented in Figure 3, can be separated into three different groups (30−225 cm^{-1}, 230−425 cm^{-1}, and 450−800 cm^{-1}). A visual inspection of spectra reveal that more than 6 number of modes are present and some modes are overlapped, unlike well-resolved modes seen in rare-earth-based pyrochlores.[32,33] To resolve the spectra into modes, least-squares fitting with sum of the Lorentzian curves is carried out. A good fit was obtained with 13 curves (Figure 3). The parameters obtained from the fit (wavenumber of the mode (ν), integrated intensity (I) and full width half maxima (fwhm)) are presented in Table 3. The Raman mode assignment of the BFT pyrochlore is carried out by comparing the wave numbers of modes with the modes reported in literature for different disordered bismuth pyrochlores.[26,34]

In the low-wavenumber range of 30−225 cm^{-1}, the BFT modes, observed at 68 and 177 cm^{-1}, were assigned to F_{1u} infrared vibrations (O′−A−O′ bend and A−BO_6 stretch) that appear in the Raman spectrum due to the relaxation of selection rules by displacements of Bi and O′ ions from their ideal sites. These modes have been observed at 73−76 and 148−180 cm^{-1} for bismuth pyrochlores from ref 26. In the present analysis, availability of the low-wavenumber Raman data (down to 30 cm^{-1}) enabled us to identify a mode at 54 cm^{-1}. This low wavenumber mode has also been seen in the infrared spectra of bismuth pyrochlores[34] (41−56 cm^{-1}), hence it was assigned as an F_{1u} mode. The

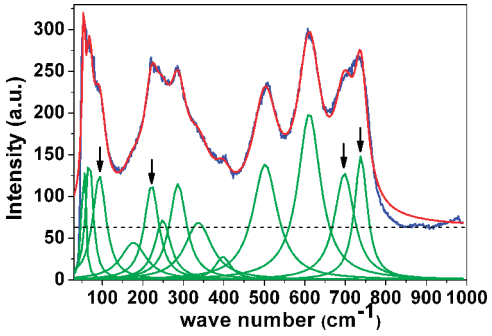

Figure 3. Sum of Lorentzian curves fit of the Raman spectra. Experimentally measured spectra (blue), fitted curve (red), baseline (broken line), and Raman modes (green) from the fit are shown. Unassigned modes are indicated by arrow marks.

modes observed at 93 and 222 cm^{-1} do not match with literature, therefore they were not assigned to any vibrations. These low-wavenumber modes, which are absent in pyrochlores with an ideal arrangement of atoms,[35,36] are consistently seen in bismuth[27,37−39] and rare-earth pyrochlores,[40] with displaced A-site ions indicating their association with the ion displacement.

In the mid-wavenumber range, the lowest mode was observed at 249 cm^{-1} and, according to ref 22, identified as F_{2g}. The two well-resolved modes at 287 and 337 cm^{-1} were assigned to E_g and F_{2g} modes, respectively. The low-intensity mode at 398 cm^{-1} is most probably another F_{2g} mode, as it close to what have been observed for $Bi_2Ti_2O_7$.

The modes in the high wavenumber range of 450−800 cm^{-1} are mostly due to the vibrations of the BO_6 octahedral with 501 cm^{-1} mode assigned as A_{1g} and 611 cm^{-1} as the F_{2g}. The 611 cm^{-1} mode may also be affected by the infrared F_{1u} mode (B−O stretch) previously observed between 599 and 642 cm^{-1}.[41] The modes above 625 cm^{-1} are generally treated as overtones in the bismuth pyrochlores but the 739 cm^{-1} mode may also be attributed to the highest F_{2g} mode, as in ref 22.

In summary, the high number of modes in the Raman spectra of the BFT pyrochlore cannot be assigned to a cubic pyrochlore with an ideal ion setting. These modes appear as a result of the relaxation of selection rules cause by lowering of the cell symmetry due to the displacive disorder. This supports our diffraction studies and selection of the 32*e* structural model for the BFT pyrochlore.

Dielectric Studies. Room-temperature dielectric constant of the BFT pyrochlore is 45 at 1 MHz and it is low compared to other Bi-based pyrochlores with d^0 ions such as Nb^{5+} and Ta^{5+} but similar to the dielectric constant of pyrochlore material with d^{10} cations, i.e., $(Bi_{1.5}Zn_{0.5})(Zn_{1.5}Sb_{0.5})O_7$. The reported dielectric constant at 1 MHz for $(Bi_{1.5}Zn_{0.5})(Zn_{1.5}Nb_{0.5})O_7$, $(Bi_{1.5}Zn_{0.5})(Zn_{1.5}Ta_{0.5})O_7$ and $(Bi_{1.5}Zn_{0.5})(Zn_{1.5}Sb_{0.5})O_7$ pyrochlores are 150, 76 and 32, respectively.[41] The study of Melot et al.[42] showed that the dielectric constant depends on the d^0 /d^{10} nature of the cation. The gradual decrease in the dielectric constant with decrease in d^0/d^{10} metal ion ratio was also reported for $(Bi_{1.5}Zn_{0.5})(Zn_{0.5-x/3}Sn_xNb_{1.5-2x/3})O_7$ pyrochlores[43] and $La(Mg_{0.5}Ti_{0.5-x}Sn_x)O_3$ perovskites.[44]

The frequency and temperature dependence of dielectric constant and dissipation (tanδ) of the BFT pyrochlore samples are presented in Figure 4. The observed dielectric characteristics closely correspond to the characteristics of dielectric relaxations observed for other displacive pyrochlores.[6,39,45] The dissipation that occurs at cryogenic temperature is broad and frequency dispersive. Its peak position ($T_{mtan\delta}$) increases from 92 to 125 K and the peaks broaden with the increase in frequencies (1 kHz-1 MHz) resembling an relaxor-like mechanism. From Figure 4 we can also see an increase in tanδ above 225 K, which is more significant

Table 3. Tentative Assignment and Fitting Parameters Obtained from Sum of Lorentzians for $(Bi_{1.88}Fe_{0.12})(Fe_{1.42}Te_{0.58})O_{6.87}$, Frequencies Calculated for $Bi_2Ti_2O_7$, Modes and Assignment Reported for Bismuth Pyrochlores

frequency (cm^{-1})	integrated intensity (a.u.)	fwhm (cm^{-1})	$Bi_2Ti_2O_7$: ref 22 mode: (cm^{-1})	Bi-pyrochlore: ref 22 mode: (cm^{-1})	tentative assignment
54	178	9.39			F_{1u}
68	149	21.3	F_{1u}: 86	F_{1u}: 73−77	F_{1u}
93	125	39.8			unassigned
177	45	76.9	F_{1u}: 142	F_{1u}: 148−180	F_{1u}
222	113	42.9			unassigned
249	72	48.1	F_{2g}: 262	F_{2g}: 208−256	F_{2g}
287	115	50.7	E_g: 281	$E_g + F_{2g}$: 297−346	E_g
337	68	80.5			F_{2g}
398	27	47.6	F_{2g}: 395	F_g: 419−434	F_{2g}
502	139	74.3	A_{1g}: 535	A_{1g}: 511−540	A_{1g}
611	199	68.2	F_{2g}: 537	F_{2g}: 599−624	F_{2g} + (F_{1u}?)
698	127	59.8			unassigned
738	148	38.4	F_{2g}: 711		unassigned

dx.doi.org/10.1021/cm200281z |*Chem. Mater.* 2011, 23, 2619–2625

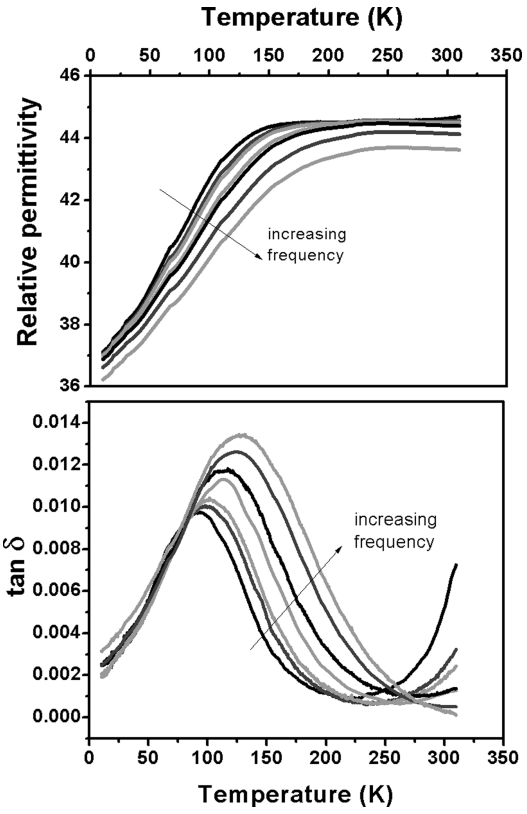

Figure 4. Temperature dependence of (a) permittivity and (b) dielectric loss (tan δ) of $(Bi_{1.88}Fe_{0.12})(Fe_{1.42}Te_{0.58})O_{6.87}$ at frequencies of 1, 5, 10, 50, 100, and 500 kHz and 1 MHz (left to right). The dispersion of the permittivity with frequency, observed for 500 kHz and 1 MHz, is an artifact due to impedance of the measurement fixture in the cryocooler.

for low frequencies and typical for system with a high concentration of charge carriers, i.e., increased conductivity.

If we assume for the displaced ions in this disordered system an independent and uniform hopping mechanism, in which the charges hop independently over a charge barrier with no correlation between the dipole entities, the thermodynamics of the relaxation time and activation energy of the hopping can be expressed by Arrhenius expression;

$$\tau = \tau_0 \exp(E_a/k_B T) \quad (1)$$

where τ_0 is the pre-exponential term, E_a the activation energy for hopping between adjoining potential minima, and k_b the Boltzmann constant. The Arrhenius plot of $\ln(\tau) = \ln(\omega^{-1})$ followed a linear variation with the $1000/T_{mtan\delta}$ resulted in the activation energy of 200 meV and the relaxation time of 7×10^{-16} s. The E_a and relaxation time are close to values typical for ion hopping. Because of very broad relaxation peak our system is most probably a more complex than one singular Debye relaxation. We can assume that a contribution of dipole fluctuation originating from the multiwall hopping of displaced Fe^{3+}, Bi^{3+} and O′ ions is dominating the relaxation.[39,46] Because the freezing temperature of the relaxation is close to zero the difference between applying Arrhenius or Vogel-Fulcher expression is not so significant that we can judge on collective nature of the fluctuation. In addition, it is important to refer to Liu et al.[47] suggestion of a possible tetrahedral edge rotation as a additional contribution to the dipole moment, which they claim for $(Bi_{1.67}Ni_{0.25})(Ni_{0.5}Nb_{1.5})O_7$. However, based on our Raman

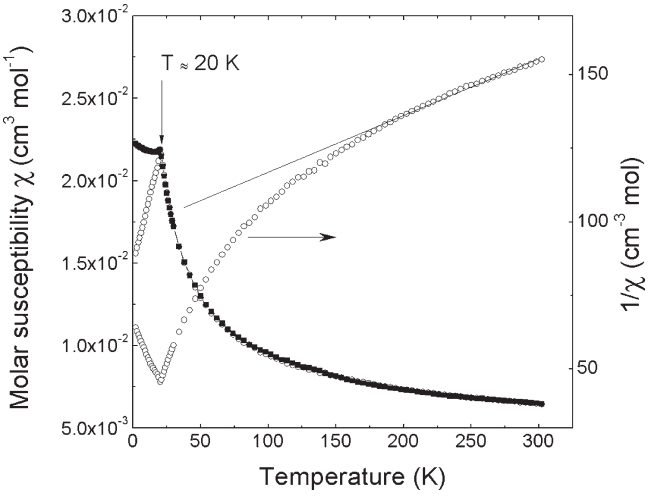

Figure 5. Temperature dependence of zero-field-cooled (open circles) and field-cooled (solid circles) molar magnetic susceptibility of the $(Bi_{1.88}Fe_{0.12})(Fe_{1.42}Te_{0.58})O_{6.87}$. Also shown is inverse magnetic susceptibility measured in magnetic field of 50 Oe.

analysis that indicates the high displacive disorder, we assume the ion hopping to be the main contributor.

Magnetic Studies. Magnetic properties of the pyrochlores were measured at various magnetic fields using zero-field cooled (ZFC) and field-cooled (FC) conditions. Magnetic susceptibility, χ, and inverse magnetic susceptibility, $1/\chi$, of BFT, measured in low magnetic field of 50 Oe, are shown in Figure 5. The χ (T) dependence shows a cusp at $T \approx 20$ K which, during the early stages of this work, was assigned to the antiferromagnetic (AFM) type of the phase transition. This preliminary assignment, however, was not confirmed by the neutron diffraction measurements both above and below 20 K that provided no evidence for the long-range magnetic order in the BFT pyrochlore. Any magnetic interaction must be very short-range, as diffuse magnetic scattering is also absent. Also specific heat measurements reveal no peak or noticeable anomalies around T = 20 K that may be associated with the magnetic entropy related to the formation of the long-range FM or AFM order further supporting the notion that the material is a spin glass system (Figure 6). Subsequent magnetic measurements reveal colossal broadening and red-shift of the χ (T) cusp in stronger magnetic fields (Figure 7). These phenomena are typically observed in the spin-glass systems.[48] In addition, it was noticed that magnetic moment below 20 K shows significant time dependence suggesting a very slow spin dynamics in agreement with the general features of the spin glass systems.[49]

Extrapolation of the linear $1/\chi$ (T) dependence in Figure 5 to $1/\chi = 0$ yields a negative Weiss temperature of $\Theta_W = -659$ K indicating that the short-range AFM superexchange interactions in the studied compounds are quite strong. In the reported literature, antiferromagnetic-type interaction in Bi-based pyrochlores, such as $Bi_{1.72}Fe_{1.06}Nb_{1.13}O_7$, was also evidenced by the negative intercepts of inverse susceptibility with Θ_W values as low as −278 K.[9]

As revealed in Figure 5, above $T \approx 250$ K the $1/\chi$ data can be fit to the Curie−Weiss law,

$$\chi = \frac{N_A p^2 \mu_B{}^2}{3k_B(T - \Theta_W)} \quad (2)$$

where N_A is the Avogadro number, p is the effective magnetic moment in Bohr magnetons (μ_B), k_B is the Boltzmann constant, and T is the absolute temperature. The fit of the $1/\chi$ data gives Fe^{3+} effective magnetic moment of ∼5 μ_B. This is somewhat lower than the noninteracting free Fe^{3+} value of 5.9 μ_B. A strong deviation from the linear Curie−Weiss behavior (eq 2)

dx.doi.org/10.1021/cm200281z |Chem. Mater. 2011, 23, 2619–2625

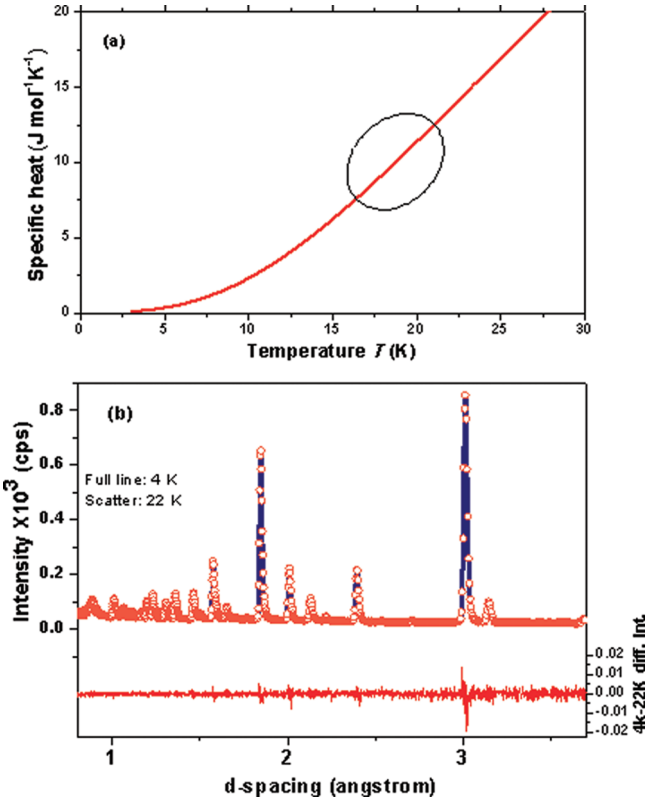

Figure 6. (a) Specific heat of the $(Bi_{1.88}Fe_{0.12})(Fe_{1.42}Te_{0.58})O_{6.87}$ sample. The data do not show any anomaly around 20 K that can be attributed to the onset of the long-range AFM or FM magnetic order. This corresponds to (b) insignificant difference (line at bottom) between neutron diffraction data collected at 4 and 22 K.

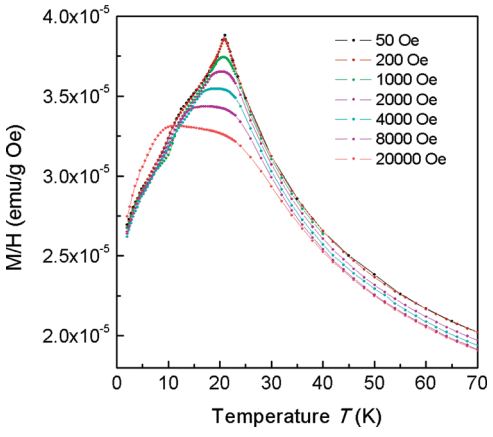

Figure 7. Temperature dependence of zero-field-cooled magnetic moment of the $(Bi_{1.88}Fe_{0.12})(Fe_{1.42}Te_{0.58})O_{6.87}$ taken in various magnetic fields.

observed below $T \approx 250$ K may point on to the presence of the weaker ferromagnetic-type interactions presumably stemming from the next nearest neighbor Fe^{3+}—Fe^{3+} spin coupling. This situation is different from the rare-earth magnetic pyrochlores,[8] where strong localization of electrons on the rare earth ions satisfies the noninteracting spin picture above the temperature of the long-range magnetic ordering.

We have also analyzed magnetoelectric properties of this pyrochlore at cryogenic temperatures. Although we have not seen any noticeable

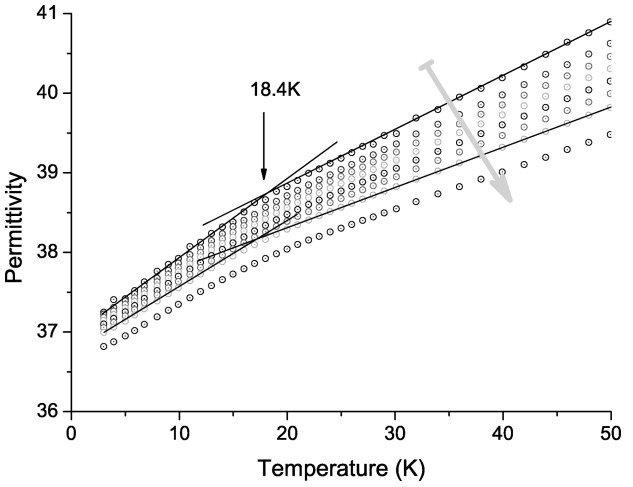

Figure 8. Permittivity at cryogenic temperatures showing frequency dependent slope change at around 19 K, which coincides with spin-glass transition temperature. The gray arrow indicates the increase in measurement frequency from 1 kHz to 1 MHz. The cooling rate during measurement was 1 K/min.

magnetic field dependence of the dielectric properties, we have noticed a gradual change in slope in the permittivity at around 19K (Figure 8). The magnitude of the slope change is frequency dependent. At the moment, it is not clear whether this anomaly is connected with the spin-glass transition, T_g, that occurs at almost the same temperature.

CONCLUSIONS

We have synthesized a new member of Bi-pyrochlore family with the highest percentage of Fe^{3+} ion, $(Bi_{1.88}Fe_{0.12})(Fe_{1.42}Te_{0.58})O_{6.87}$. Observation of the (442) reflection in the X-ray and neutron powder diffraction pattern indicates that the pyrochlore crystallizes with displaced atomic A-sites similar to other Bi-based misplaced-displacive pyrochlores. A structure refinement of the X-ray and neutron diffraction data reveal that the A-site is displaced to 96*g* and O′ site is displaced to 32*e* in cubic $Fd\bar{3}m$ symmetry. The refinement results indicate that ~6% of the Fe^{3+} is misplaced on the A-site. The Raman spectrum was modeled with 13 Lorentzian peaks and a possible assignment of modes based on the literature data was carried out. The higher number of Raman modes together with the presence of the low-wavenumber modes confirm the displacive nature of the $(Bi_{1.88}Fe_{0.12})(Fe_{1.42}Te_{0.58})O_{6.87}$. The dielectric characterization shows on a frequency diffusive and dispersive dielectric relaxation at around 120 K that originates in multiwall hopping of displaced ions. Room temperature dielectric constant of $(Bi_{1.88}Fe_{0.12})(Fe_{1.42}Te_{0.58})O_{6.87}$ is 45 at 1 MHz. The increasing permittivity and dielectric losses, observed above 225 K, indicate on increased conductivity of the pyrochlore at room temperature. At 20 K, the pyrochlore develops a strong spin interactions resulting in spin-glass phase transition.

ASSOCIATED CONTENT

Supporting Information. Crystallographic information file (CIF). This material is available free of charge via the Internet at http://pubs.acs.org.

AUTHOR INFORMATION

Corresponding Author

*E-mail: matjaz.valant@ung.si.

Present Addresses

‡Light Scattering Laboratory, Chemistry and Physics of Materials Unit, Jawaharlal Nehru Centre for Advanced Scientific Research, Jakkur, Bangalore 560 064, India.

ACKNOWLEDGMENT

The authors thank Hiroya Sakurai for valuable comments on spin-glass properties. This work has benefited from the use of HIPD at the Lujan Center at Los Alamos Neutron Science Center, funded by DOE Office of Basic Energy Sciences. Los Alamos National Laboratory is operated by Los Alamos National Security LLC under DOE Contract DE-AC52-06NA25396.

REFERENCES

(1) Ewing, R. C.; Weber, W. J.; Lian, J. *J. Appl. Phys.* **2004**, *95*, 5949.
(2) Kayed, T. S.; Mergen, A. *Cryst. Res. Technol.* **2003**, *38*, 1077.
(3) Kim, I. D.; Choi, Y. W.; Tuller, H. L. *Appl. Phys. Lett.* **2005**, *87*, 043509.
(4) Subramanyam, M. A.; Aravamudan, G.; Subba Rao, G. V. *Prog. Solid State Chem.* **1983**, *15*, 55.
(5) Cann, D. P.; Randall, C. A.; Shrout, R. A. *Solid State Commun.* **1996**, *1006*, 529.
(6) Valant, M.; Davies, P. K. *J. Am. Ceram. Soc.* **2000**, *83*, 147.
(7) Lu, J.; Klenov, D. O.; Stemmer, S. *Appl. Phys. Lett.* **2004**, *84*, 957.
(8) Gardner, J. S.; Gingras, M. J. P.; Greedan, J. E. *Rev. Mod. Phys.* **2010**, *82*, 53.
(9) Lufaso, M. W.; Vanderah, T. A.; Pazos, I. M.; Levin, I.; Roth, R. S.; Nino, J. C.; Provenzano, V.; Schenck, P. K. *J. Solid State Chem.* **2006**, *179*, 3900.
(10) Vanderah, T. A.; Siegrist, T.; Lufaso, M. W.; Yeager, M. C.; Roth, R. S.; Nino, J. C.; Yates, S. *Eur. J. Inorg. Chem.* **2006**, 4908.
(11) Filoti, G.; Rosenberg, M.; Kuncser, V.; Seling, B.; Fries, T.; Spies, A.; Kemmler-Sack, S. *J. Alloys and Comp.* **1998**, *268*, 16.
(12) Baettig, P.; Ederer, C.; Spaldin, N. A. *Phys. Rev. B.* **2005**, *72*, 214105.
(13) Selbach, S. M.; Tybell, T.; Einarsrud, M.-A.; Grande, T. *Chem. Mater.* **2009**, *21*, 5176.
(14) Weller, M. T.; Hughes, R. W.; Rooke, J.; Knee, C. S.; Reading *J. Dalton Trans.* **2004**, 3032.
(15) Tabira, Y.; Withers, R. L.; Yamada, T.; Ishizawa, N. Z. *Kristallogr.* **2001**, *216*, 92.
(16) Levin, I.; Amos, T. G.; Nino, J. C.; Vanderah, T. A.; Randall, C. A.; Lanagan, M. T. *J. Solid State Chem.* **2002**, *168*, 69.
(17) Shoemaker, D. P.; Seshadri, R.; Tachibana, M.; Hector, A. L. arXiv:1101.0791v1 [cond-mat.mtrl- sci] 4 Jan 2011
(18) Shoemaker, D. P.; Seshadri, R.; Hector, A. L.; Llobet, A.; Proffen, T.; Fennie, C. J. *Phys. Rev. B.* **2010**, *81*, 144113.
(19) Krayzman, V.; Levin, I.; Woicik, J. C *Chem. Mater.* **2007**, *19*, 932.
(20) Avdeev, M.; Haas, M. K.; Jorgensen, J. D.; Cava, R. J. *J. Solid State Chem.* **2002**, *169*, 24.
(21) Roth, R. S.; Vanderah, T. A.; Bordet, P.; Grey, I. E.; Mumme, W. G.; Cai, L.; Nino, J. C. *J. Solid State Chem.* **2008**, *181*, 406.
(22) Vanderah, T. A.; Levin, I.; Lufaso, M. W. *Eur. J. Inorg. Chem.* **2005**, 2895.
(23) Larson, A. C.; Von Dreele, R. B. *General Structure Analysis system (GSAS)*; Los Alamos National Laboratory Report, LAUR 86-748; Los Alamos National Laboratory: Los Alamos, NM, 2000.
(24) Toby, B. H. *J. Appl. Crystallogr.* **2001**, *34*, 210.
(25) Meneses, D. D. S.; Gruener, G.; Malki, M.; Echegut, P. *J. Non-Cryst. Solids* **2005**, *351*, 124.
(26) Arenas, D. J.; Gasparov, L. V.; Qui., W.; Nino, J. C.; Patterson., H. C.; Tanner, D. B. *Phys. Rev. B.* **2010**, *82*, 214302.
(27) Henderson, S. J.; Shebanova, O.; Hector, A. L.; McMillan, P. F.; Weller, M. T. *Chem. Mater.* **2007**, *19*, 1712.
(28) Vanderah, T. A.; Lufaso, M. W.; Alder, A. U.; Levin, I.; Nino, J. C.; Provenzano, V.; Schenck, P. K. *J. Solid State Chem.* **2006**, *179*, 3467.
(29) Hector, A. L.; Wiggins, S. B. *J. Solid State Chem.* **2004**, *177*, 139.
(30) Withers, R. A.; Welberry, T. R.; Larsson, A. K.; Liu, Y.; Norén, L.; Rundlöf, H.; Brink, F. J. *J. Solid State Chem.* **2004**, *17*, 231.
(31) McCauley., R. A. *J. Opt. Soc. Am.* **1973**, *101*, 104116.
(32) Maczka, M.; Sanjuán, M. L.; Fuentes, A. F.; Hermanowicz, K.; Hanuza, J. *Phys. Rev. B.* **2008**, *78*, 134420.
(33) Bae, J. S.; Yang, I.-S.; Lee, J. S.; Noh, T. W.; Takeda, T.; Kanno, R. *Phys. Rev. B.* **2006**, *73*, 052301.
(34) Chen, M.; Tanner, D. B.; Nino, J. C. *Phys. Rev. B* **2005**, *72*, 054303.
(35) Brown, S.; Gupta, H. C.; Alonso, J. A.; Martinez-Lope, M. J. *Phys. Rev. B* **2004**, *69*, 054434.
(36) Saha, S.; Singh, S.; Dkhil, B.; Suryanarayanan, R.; Dhalenne, G.; Revcolevschi, A.; Sood, A. K. *Phys. Rev. B* **2008**, *78*, 2104102.
(37) Wang, H.; Kamba, S.; Du, H.; Zhang, M.; Chia, C.-T.; Veljko, S.; Denisov, S.; Kadlec, F.; Petzelt, J.; Yao, X. *J. Appl. Phys.* **2006**, *100*, 014105.
(38) Liu, Y.; Withers, R. L.; Nguyen, H. B.; Elliott, K.; Ren, Q.; Chen, Z. *J. Solid State Chem.* **2009**, *182*, 2748.
(39) Kamba, S.; Porokhonskyy, V.; Pashkin, A.; Bovtun, V.; Petzelt, J.; Nino, J. C.; Trolier-McKinstry, S.; Lanagan, M. T.; Randall, C. A. *Phys. Rev. B* **2002**, *66*, 054106.
(40) Maczka, M.; Knyazev, A. V.; Kuznetsova, N. Yu.; Ptak, M.; Macalik. L, *J. Raman Spectrosc.* 2010.
(41) Huiling, D.; Xi, Y. *J. Mater. Sci. Mater. Electron.* **2004**, *15*, 613.
(42) Melot, B.; Rodriguez, E.; Proffen, Th.; Hayward, M. A.; Seshadri, R. *Mater. Res. Bull.* **2006**, *41*, 961.
(43) Du, H.; Yao, X.; Zhang, L. *Ceram. Int.* **2002**, *28*, 231.
(44) Babu, G. S.; Subramanian, V.; Murthy, V. R. K.; Lin, I. N.; Chia, C.-T.; Liu, H. L. *J. Appl. Phys.* **2007**, *102*, 064906.
(45) Valant, M. *J. Am. Ceram. Soc.* **2009**, *92*, 955.
(46) Nino, J. C.; Lanagan, M. T.; Randall, C. A. *J. Appl. Phys.* **2001**, *89*, 8.
(47) Liu., Y.; Withers, R. L.; Nguyen, B.; Wei, X. Y. *J. Aust. Ceram. Soc.* **2007**, *43*, 75.
(48) Nagata, S.; Keesom, P. H.; Harrison, H. R. *Phys. Rev. B* **1979**, *19*, 1633.
(49) Zhou, H. D.; Wiebe, C. R.; Harter, A.; Dalal, N. S.; Gardner, J. S. *J. Phys.: Condens. Matter* **2008**, *20*, 325201.